Eur. Phys. J. A (2016) **52**: 202
DOI 10.1140/epja/i2016-16202-3

THE EUROPEAN PHYSICAL JOURNAL A

Regular Article – Theoretical Physics

The Gogny-Hartree-Fock-Bogoliubov nuclear-mass model*

S. Goriely[1,a], S. Hilaire[2], M. Girod[2], and S. Péru[2]

[1] Institut d'Astronomie et d'Astrophysique, CP-226, Université Libre de Bruxelles, 1050 Brussels, Belgium
[2] CEA, DAM, DIF, F-91297, Arpajon, France

Received: 27 April 2016 / Revised: 22 June 2016
Published online: 26 July 2016 – © Società Italiana di Fisica / Springer-Verlag 2016
Communicated by N. Alamanos

Abstract. We present the Gogny-Hartree-Fock-Bogoliubov model which reproduces nuclear masses with an accuracy comparable with the best mass formulas. In contrast to the Skyrme-HFB nuclear-mass models, an explicit and self-consistent account of all the quadrupole correlation energies is included within the 5D collective Hamiltonian approach. The final rms deviation with respect to the 2353 measured masses is 789 keV in the 2012 atomic mass evaluation. In addition, the D1M Gogny force is shown to predict nuclear and neutron matter properties in agreement with microscopic calculations based on realistic two- and three-body forces. The D1M properties and its predictions of various observables are compared with those of D1S and D1N.

1 Introduction

Astrophysical considerations require to build nuclear-mass models that have as rigorous a footing as possible (see [1] for a review on the r-process nucleosynthesis and the importance of nuclear masses). In this way one might hope to be able to extrapolate from the mass data, which cluster fairly closely to the stability line, out towards the neutron drip line, and make reliable estimates of the properties (including masses) of nuclei that are so neutron rich that there is no hope of measuring them in the foreseeable future. To this end, a series of nuclear-mass models have been developed on the basis of mean-field models. So far, only the non-relativistic Hartree-Fock-Bogoliubov (HFB) method with Skyrme and contact-pairing forces [2, 3], in which the force parameters are fitted to essentially all the experimental mass data, has led to competitive mass formulas with respect to the more traditional macroscopic-microscopic mass formula based on the liquid drop approach [4] or other global approaches [5] (the use of the term "mass formula" follows the usual designation of any semi-empirical mass model that has been fitted to essentially all mass data with a root mean square (rms) deviation typically lower than 1 MeV and for which a complete mass table, running from one drip line to the other, has been constructed). In particular, the Skyrme-HFB approach, together with phenomenological Wigner terms and correction terms for the spurious collective energy, has proven its capacity to reproduce all experimental masses [6, 7] with an rms deviation similar to or even better than the best droplet-like models [2, 3]. Although the Skyrme-HFB method has opened a new era in the construction of mass formulas, it remains to be tested with respect to other microscopic approaches, like the relativistic mean-field model or with respect to finite-range interactions, such as the Gogny interaction. Furthermore, effects beyond mean field are known to affect predictions significantly [8] but have either been crudely approximated or totally neglected in the previous mass formulas.

In this paper, we present the D1M mass formula obtained within the HFB framework with a Gogny interaction taking into account all the quadrupole correlations self-consistently and microscopically [9]. Though the existing Gogny forces like D1S [10] or D1N [11] present global properties in agreement with most observables, they are not suited for an accurate estimate of nuclear masses [11], as illustrated in fig. 1 (upper panels). In particular, D1S masses [10] give rise to a clear isotopic drift which tends to overbind neutron-deficient isotopes and underbind the neutron-rich ones by up to 10 MeV, leading to an overall rms deviation with respect to the bulk of experimental data of about 2.5–3 MeV. An improvement has been achieved with the D1N interaction [11], but systematic patterns, including arches between neutron magic numbers, remain visible (fig. 1) and show deviations with respect to measured masses significantly larger than the

* Contribution to the Topical Issue "Finite range effective interactions and associated many-body methods - A tribute to Daniel Gogny" edited by Nicolas Alamanos, Marc Dupuis, Nathalie Pillet.

[a] FRS-F.N.R.S. research associate;
e-mail: sgoriely@astro.ulb.ac.be

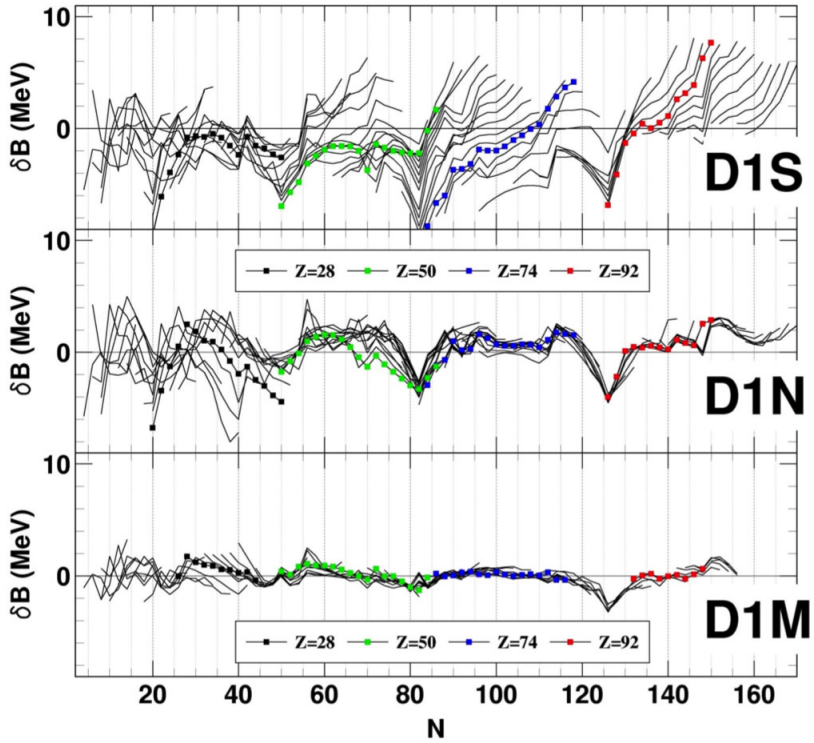

Fig. 1. (Color online) Differences between theoretical Gogny-HFB (plus 5DCH) and experimental binding energies. The upper panel is obtained with the D1S interaction, the middle panel with D1N and the lower panel with D1M. Some isotopic chains for $Z = 28$, 50, 74 and 92 are highlighted with colored circles.

Skyrme-HFB calculations which reach a 0.5–0.7 MeV rms deviation. For this reason, a new Gogny force, D1M, has been developed and fitted to all measured masses, keeping the additional constraint to provide reliable nuclear matter and neutron matter properties, but also radii, giant resonance and fission properties. In addition, for the first time the quadrupole collective corrections have been included in the mass formula by solving the collective Schrödinger equation with the 5-dimensional collective Hamiltonian (5DCH) [12, 13]. In sect. 2, we present the Gogny-HFB mass model, including the fitting strategy. The D1M properties regarding various observables related to nuclei of infinite nuclear matter are described in sect. 3 and compared with those obtained with D1S or D1N. Finally, conclusions are drawn in sect. 4.

2 The Gogny-HFB mass model

2.1 The Gogny-HFB model

The Gogny-HFB model has been described in length in various papers (see refs. [10–12, 14, 15] and references therein). Both axially and triaxially deformed HFB codes have been used to perform the calculations. These are written in terms of an expansion of the single-particle functions in a harmonic-oscillator basis. The triaxial code is used to determine the quadrupole corrections to the total binding energy and the charge radius. These are estimated within the 5DCH model [12, 13] by

$$\Delta E_{\rm quad} = E_{\rm MF} - E_{\rm BMF}, \qquad (1)$$

where $E_{\rm MF}$ is the mean-field (MF) energy obtained in the axial symmetry approximation and $E_{\rm BMF}$ is the binding energy obtained beyond the mean-field (BMF) approximation, *i.e.* including the quadrupole corrections treated with the 5DCH model. Similarly, dynamical corrections are known to affect significantly the nuclear radius. The quadrupole correction to the charge radii is estimated by

$$\Delta r_{\rm quad} = \sqrt{r^2_{\rm BMF} - r^2_{\rm MF}}\,, \qquad (2)$$

the final charge radius being estimated by $r^2_{\rm th} = r^2_{\rm MF} + \Delta r^2_{\rm quad}$. Note that the quadrupole corrections are calculated for even-even nuclei only and interpolated from those for the others, while in the HFB calculation odd nuclei are treated in the blocking plus equal filling approximation. For closed-shell nuclei, the Gaussian overlap approximation used within the 5DCH approach gives erroneous negative corrections (see ref. [13] for more details). For those nuclei, the correction is therefore set to zero.

The total binding energy reads $E_{\rm th} = E_{\rm axial} + \Delta E_{\rm quad} + \Delta E_\infty$ where in addition to the quadrupole correlations, an infinite-basis correction ΔE_∞ is introduced due to the limitation of the number of major shells included in the axially symmetric calculation. The same procedure as described in ref. [14] is followed to estimate ΔE_∞. If the energy $E_{\rm axial}$ obtained with the axial code using $N \lesssim 14$ major shells can be determined within a reasonable computation time, this is not the case for both ΔE_∞ and $\Delta E_{\rm quad}$ (see also ref. [16] for a detailed study of the convergence of the calculations with respect to the basis dimension).

Therefore, to avoid unfeasible calculations, the adjustment of the Gogny force parameters to reproduce at best the experimental masses is not performed by systematically calculating these correction terms. Instead, the computational scheme described below is followed.

2.2 Fitting strategy

A mass fit entails that every nucleus that is included in the fit has to be calculated many times over. Making a direct fit with a deformed HF code to all of the more than 2000 measured masses is extremely computer-time consuming, so that in practice a specific strategy needs to be followed, especially in view of the large number of free parameters (typically 14) and the many observables that need to be fitted. The Gogny effective nuclear interaction (plus spin-orbit term) is expressed [10] as

$$V(1,2) = \sum_{j=1,2} e^{-\frac{(\mathbf{r}_1-\mathbf{r}_2)^2}{\mu_j^2}} (W_j + B_j P_\sigma - H_j P_\tau - M_j P_\sigma P_\tau) + t_0 \left(1 + x_0 P_\sigma\right) \delta\left(\mathbf{r}_1 - \mathbf{r}_2\right) \left[\rho\left(\frac{\mathbf{r}_1 + \mathbf{r}_2}{2}\right)\right]^\alpha + i\, W_{LS} \overleftarrow{\nabla}_{12} \delta\left(\mathbf{r}_1 - \mathbf{r}_2\right) \times \overrightarrow{\nabla}_{12} \cdot \left(\overrightarrow{\sigma}_1 + \overrightarrow{\sigma}_2\right),$$

where P_σ (P_τ) is the two-body spin- (isospin-) exchange operator. From the 14 interaction parameters, it is possible to express [15] the parameters of symmetric infinite nuclear matter (INM) at the equilibrium density ρ_0 (or equivalently the Fermi momentum $k_\mathrm{F} = (3/2\,\pi^2\rho_0)^{1/3}$), namely the energy per nucleon a_v, the symmetry coefficient J, the effective mass m^* and the incompressibility coefficient K_v. These five parameters are explicitly introduced in the fits instead of 5 of the Gogny force parameters. Starting from a trial force providing a first estimate of ΔE_quad and ΔE_∞, the following 3-step iterative procedure is adopted:

i) The 5 INM parameters as well as the spin-orbit parameter W_{LS} are adjusted through an automatic optimization procedure to minimize the rms deviation with respect to experimental masses [7]; the 5 INM parameters are however kept within their corresponding experimental ranges [2,11].

ii) The remaining parameters (only the α and x_0 parameters are kept fixed) are manually adjusted to optimize quantitatively the rms deviation with respect to known charge radii [17] (in practice, this corresponds essentially to a modification of k_F) and qualitatively to the energy density curves of the infinite neutron matter (to agree with the realistic calculation of [18]) and symmetric matter in the four spin-isospin channels to agree qualitatively with [19–21]. Any modification at this stage is fed back into step (i) to ensure an optimum mass prediction.

iii) As soon as an acceptable reproduction of all the abovementioned observables is achieved, the ΔE_quad and ΔE_∞ correction energies are re-estimated and the new force is fed back into step i). A new iteration cycle begins until all the conditions are properly fulfilled with one unique force.

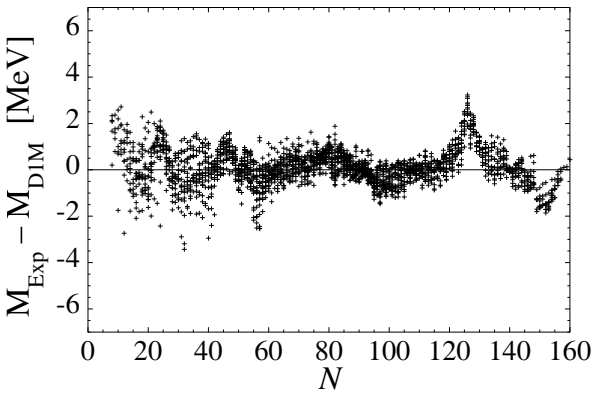

Fig. 2. Differences between measured [7] and D1M masses, as function of the neutron number N.

Table 1. Rms (σ) and mean ($\bar{\epsilon}$) deviations between data and D1M predictions (energies in MeV, radii in fm).

	σ	$\bar{\epsilon}$
2149 masses (vs AME03) [6]	0.798	0.126
2352 masses (vs AME12) [7]	0.789	0.103
2185 masses with $\lvert N-Z\rvert > 2$ [7]	0.766	0.132
2198 neutron binding energies [7]	0.523	0.012
2064 β-decay energies [7]	0.646	−0.004
792 charge radii [17]	0.032	−0.005

3 Results

3.1 Mass-related properties

The parameters of the D1M Gogny force can be found in ref. [9]. The deviations between all the 2353 measured masses [7] and the new D1M predictions are shown in fig. 2. The rms values of these deviations are given in table 1. In particular, the rms deviation on masses with respect to the 2012 mass evaluation (AME12) [7] amounts to 0.789 MeV, about 10 keV less in comparison with the rms deviation with respect to the 2003 mass evaluation (AME03) [6] to which the D1M was initially fitted. The predictions have consequently been relatively stable or even improved when adding the 203 newly measured nuclei. The same holds for the D1M neutron binding energies and β-decay Q-values which better describe the 2012 data in comparison with those used in 2003. The D1M accuracy is also comparable to the best available nuclear mass formulas and by far better than the one obtained with previous Gogny forces, like D1S and D1N (see fig. 1).

It should be noted that in the Gogny-HFB calculation, no Wigner correction for $N \simeq Z$ nuclei has been included, in contrast to what is done in the Skyrme-HFB approach. If we only consider the 2000 nuclei with $\lvert N-Z\rvert > 2$, the rms deviation drops to 0.766 MeV. As shown in fig. 2, no deviation exceeds 3.2 MeV. However, like in all Skyrme-HFB mass formulas, the highest deviations occur around magic numbers, in particular masses in the $N \simeq 126$ region remain significantly overbound. The inclusion of the particle-vibration coupling effects, known to modify the

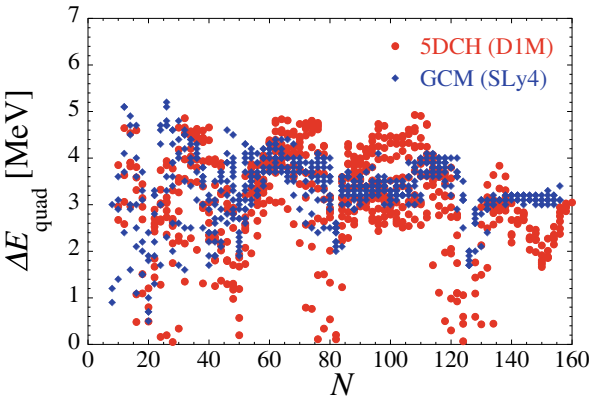

Fig. 3. (Color online) 5DCH quadrupole correction energies with D1M as a function of the neutron number N for the even-even nuclei with known masses. Also shown for comparison are the GCM quadrupole energies with SLy4 Skyrme interaction [24].

single-particle level density at the Fermi energy and consequently the amplitude of the shell effect, could change this trend [22,23].

The quadrupole correction energies obtained self-consistently within the 5DCH approach with the D1M interaction are shown in fig. 3. They amount to no more than 5 MeV, but remain sensitive to the interaction, in particular to the pairing strength and the effective mass. The quadrupole corrections obtained with different interactions typically affect the rms deviation by a few hundred keV. This remains relatively large with respect to the mass model accuracy, so that it is mandatory to recalculate self-consistently, *i.e.* with the same interaction as used in the mean-field part, the corrections at the end of a fitting iteration. The quadrupole correction energies are also compared in fig. 3 with those obtained within the General Coordinate Method (GCM) with the SLy4 Skyrme interaction [24]. The amplitude is rather similar in both cases, though patterns are clearly different for open-shell nuclei. The GCM approach also has the advantage of being applicable around closed shells. The GCM quadrupole energies have been determined with the D1M interaction in ref. [16] and are found to be about 2 MeV larger than the 5DCH predictions. The use of the GCM quadrupole energies would therefore require a re-adjustment of the Gogny interaction to fit the nuclear masses. The computer time demanded by the GCM remains unfortunately relative high compared with the 5DCH approach, but in the future it might become feasible to develop a mass model based on the GCM quadrupole corrections. Similarly, octupole correction energies estimated within the GCM with the D1M interaction have been shown to be non-negligible and as large as 2.5 MeV [25,26] and could be included in future mass models.

3.2 INM properties

The corresponding INM parameters are compared in table 2 with those characterizing the D1S and D1N interactions. Although saturation is found at more or less the same density, these interactions are characterized by a quite different volume term a_v, symmetry energy J, incompressibility K_v and effective masses m^*. We compare in fig. 4 the low-density equation of state (EoS) in pure neutron matter and symmetric nuclear matter obtained

Table 2. INM parameters for D1S, D1N, and D1M at equilibrium density ρ_0. G_0 and G'_0 are the corresponding Landau parameters [15].

	D1S	D1N	D1M
ρ_0 [fm^{-3}]	0.163	0.161	0.165
k_F [fm]	1.342	1.336	1.346
a_v [MeV]	−16.011	−15.962	−16.026
J [MeV]	31.12	29.59	28.55
m^*/m	0.697	0.748	0.746
K_v [MeV]	202.9	225.6	225.0
G_0	0.47	0.76	−0.01
G'_0	0.63	0.38	0.71

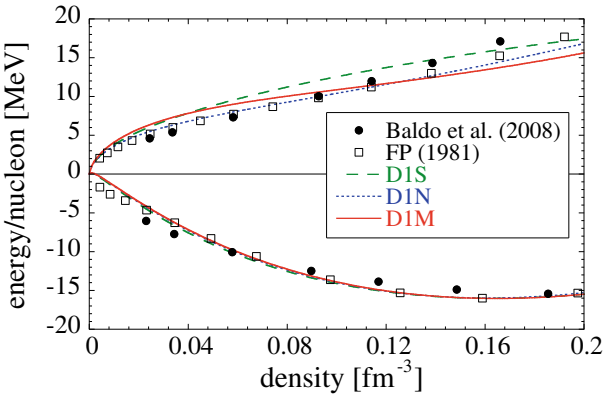

Fig. 4. (Color online) Low-density zero-temperature EoS in pure neutron matter and in symmetric nuclear matter of D1S, D1N, and D1M interactions. The predictions are compared with the calculations of refs. [18,19].

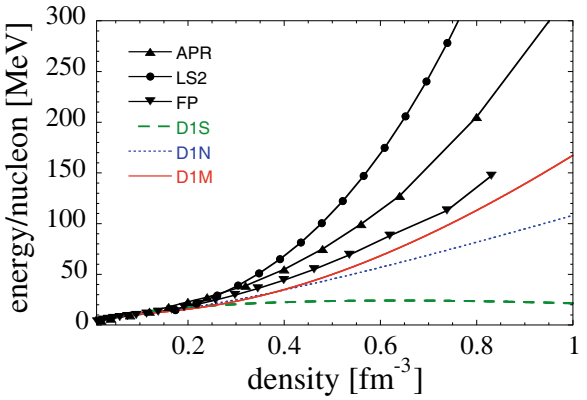

Fig. 5. (Color online) High-density zero-temperature EoS in pure neutron matter for D1S, D1N, and D1M. LS2 corresponds to the realistic EoS referred to as V18 in ref. [20]; FP and APR are the EoS of refs. [18] and [27], respectively.

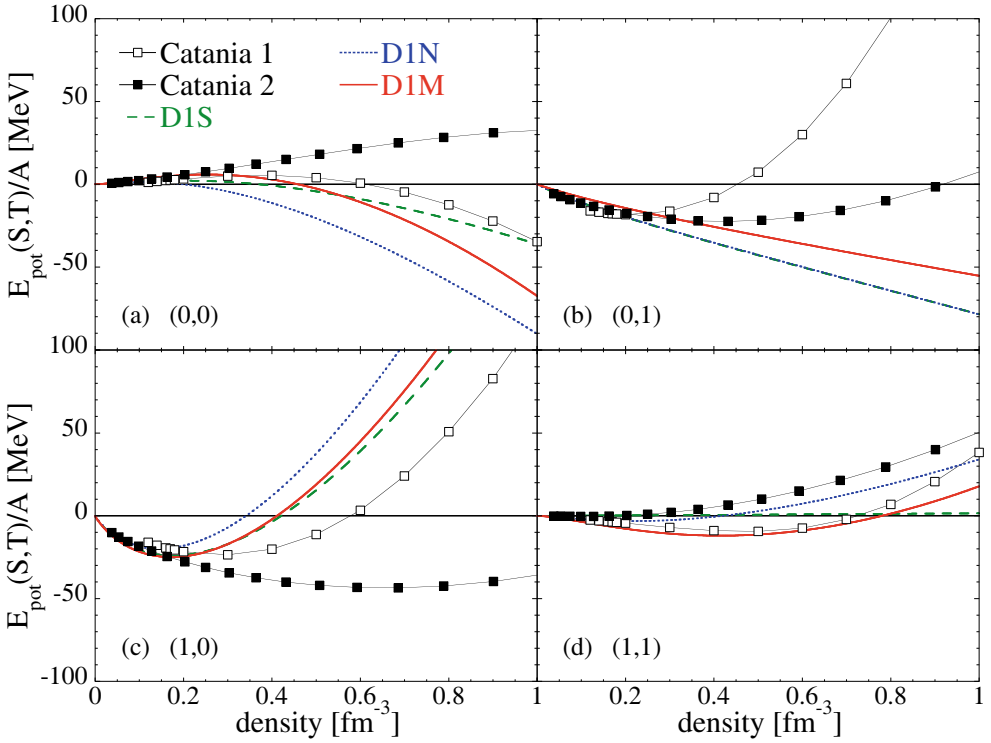

Fig. 6. (Color online) Potential energy per particle $E_{\rm pot}/A$ in each (S,T) channel for the three interactions D1S, D1N, and D1M as a function of density for charge-symmetric INM. The open symbols correspond to the "Catania 1" BHF calculations [20], and the solid symbols to the "Catania 2" BHF calculations [21].

with the D1S, D1N and D1M interactions with the realistic calculations of refs. [18,19]. A rather satisfactory description is found. In fig. 5, the EoS in pure neutron matter is shown in the high-density region, up to $1\,\mathrm{fm}^{-3}$ and compared with the Brueckner-Hartree-Fock (BHF) EoS of Friedman and Pandharipande [18] (FP), Akmal *et al.* [27] labeled "A18 + $\delta\,v$ + UIX*", and we refer to as APR, and the EoS labeled "V18" in ref. [20], which we refer to as LS2. These three EoS illustrate the relatively wide range of predicted EoS at high densities. The Gogny EoS is seen to be relatively soft with respect to the realistic calculations. While D1M follows rather well the FP density dependence, D1S leads to a collapse of neutron star matter.

3.3 Distribution of potential energy among the (S, T) channels

Figure 6 shows the potential energy per particle for symmetric nuclear matter in each of the four two-body spin-isospin (S,T) channels for the three interactions D1S, D1N, and D1M and compares them with two different BHF calculations with realistic two- and three-nucleon forces: "Catania 1", based on ref. [20] and "Catania 2", based on ref. [21]. Note that the BHF calculations are still affected by non-negligible uncertainties (see for example [28]), so that only qualitative conclusions from such a global comparison of the interaction can be drawn. In this respect, a fair agreement between D1M and the realistic calculations can be seen in all states, in particular the repulsive nature of the $(S=0,T=0)$ state that is usually not reproduced by effective Skyrme interactions [28]. Similarly, both D1N and D1M reproduce rather well the density dependence of the $(S=1,T=1)$ channel, in contrast to D1S. However, a different density dependence is found at high density in the even-singlet $(S=0,T=1)$ channel which is constrained by the pairing.

3.4 Effective masses

In contrast to D1N predictions, we obtain with D1M the correct sign for the isovector splitting of the effective mass for neutron-rich matter, *i.e.* a higher neutron than proton effective mass $m^*_n > m^*_p$ at all positive asymmetries, as shown in fig. 7. Such an isovector splitting of the effective mass is consistent with measurements of isovector giant resonances [28], and confirmed in several many-body calculations with realistic forces [29].

3.5 Collective excitations

The D1M force has also been tested with respect to various additional observables, such as the kinetic moment of inertia in Er or Pu nuclei, the giant monopole, dipole and quadrupole energy in ^{208}Pb calculated within the random-phase approximation (see table 3), and the 5DCH energy of the lowest 2^+ levels for the 519 even-even nuclei for

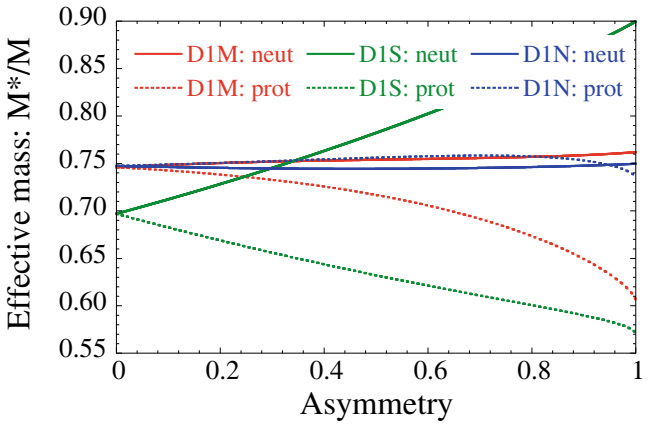

Fig. 7. (Color online) Comparison of the neutron and proton effective masses at saturation density as a function of the asymmetry of INM for the D1S, D1N, and D1M interactions.

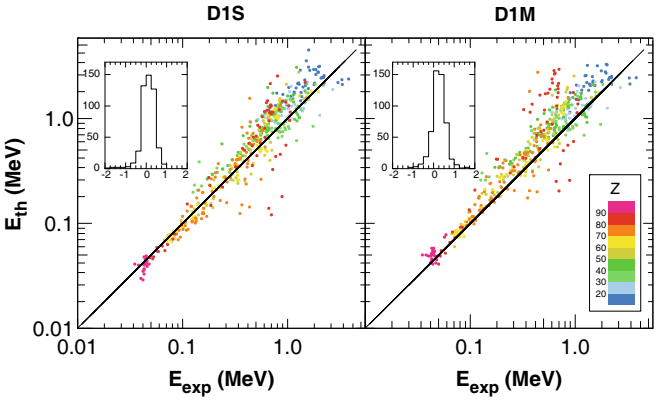

Fig. 8. (Color online) Comparison between D1S (left panel) and D1M (right panel) 2_1^+ excitation energies with experimental data [30,31] for some 519 even-even nuclei. The inset show the resulting distributions around experimental data.

which experimental data is available [30, 31] (see fig. 8). Details about the formalism and numerical calculations can be obtained in ref. [12, 13]. For all these observables, D1M and D1S give very similar results.

It has also been shown in ref. [32] that D1M gives systematically GDR centroid energies that are a few hundred keV lower than D1S, as illustrated in fig. 9.

Table 3. ^{208}Pb giant monopole (GMR), dipole (GDR) and quadrupole (GQR) resonance energies (in MeV) compared with experimental data for D1S, D1N and D1M.

	D1S	D1N	D1M	Exp.
GMR	13.37	14.18	14.25	14.17 [33]
GDR	16.37	14.50	15.85	13.43 [34]
GQR	11.98	11.99	12.14	10.60 [35]

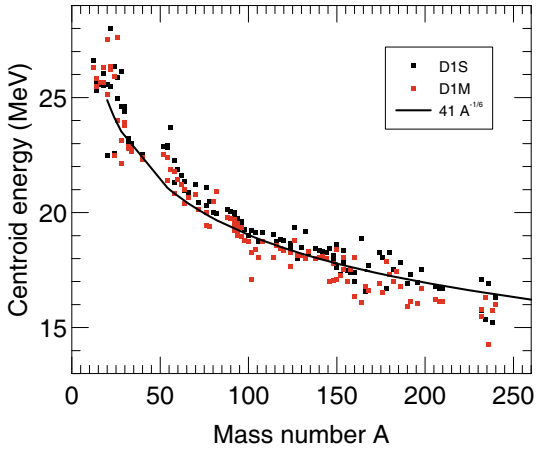

Fig. 9. (Color online) Energies of the centroid of the QRPA $B(E1)$ distributions calculated with D1S and D1M Gogny interactions for all the nuclei considered in this work. The full line represents a general fit to the points.

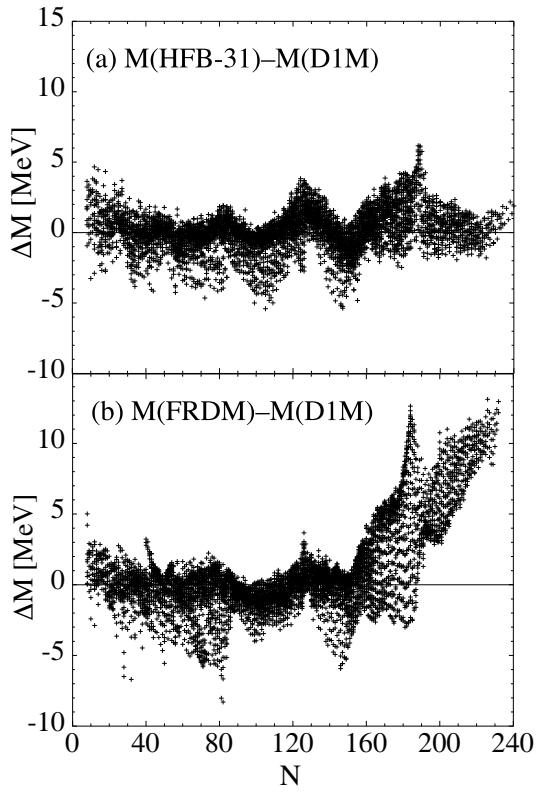

Fig. 10. Differences between (a) HFB-31 [3] and D1M masses and (b) FRDM [4] and D1M masses for all $Z, N \geq 8$, $Z \leq 110$ nuclei between the proton and neutron drip lines.

3.6 Mass extrapolations

In fig. 10, we compare the D1M predictions with those of the latest Skyrme-HFB model (HFB-31) [3] and of the finite-range droplet model (FRDM) [4]. In both cases we see that despite the close similarity in the quality of the fits to the data given by these different models, large differences can emerge, especially for heavy nuclei ($Z > 80$) and as the neutron-drip line is approached ($N > 160$). The

mass difference between HFB-31 and D1M remains however within ± 5 MeV for all the ~ 7000 $Z, N \geq 8$, $Z \leq 110$ nuclei between the proton and neutron drip lines included in the comparison.

Finally, note that many D1M properties of the ground and excited states of heavy nuclei with $92 \leq Z \leq 104$ have been studied in ref. [36] and compared with experiment, non-relativistic Skyrme HFB as well as relativistic mean-field calculations. These include in particular single-particle spectra, odd-even mass staggering and moments of inertia.

4 Conclusions

We have described the Gogny-HFB nuclear-mass model based on the D1M interaction and compared its properties to those obtained with the D1S and D1M interactions. The rms deviation with respect to essentially all the available mass data has been reduced from typically a few MeV with previous interactions to less than 0.8 MeV. Furthermore, the mass formula takes an explicit and self-consistent account of all the quadrupole correlations affecting the binding energy. The quadrupole corrections are estimated microscopically on the basis of a 5-dimensional collective Hamiltonian with the same D1M interaction. Given also the constraints imposed on the Gogny force by microscopic calculations of neutron matter and symmetric nuclear matter, this new model is particularly well adapted to astrophysical applications such as the r-process of nucleosynthesis. Different improvements to the mass model should still be brought, in particular including GCM quadrupole [16] and octupole [26] correlations or generalizing the Gogny force by introducing a finite range to the density-dependent term [15]. Fission barriers also correspond to some fundamental structure properties that can shed light on the relevance of the interaction in the deformation space. Such complex calculations have already been performed with the D1M interaction [37,38] and will certainly be given more attention in the future.

References

1. M. Arnould, S. Goriely, K. Takahashi, Phys. Rep. **450**, 97 (2007).
2. S. Goriely, Nucl. Phys. A **933**, 68 (2015).
3. S. Goriely, N. Chamel, J.M. Pearson, Phys. Rev. C **93**, 034337 (2016).
4. P. Möller, J.R. Nix, W.D. Myers, W.J. Swiatecki, At. Data Nucl. Data Tables **59**, 185 (1995).
5. J. Duflo, A.P. Zuker, Phys. Rev. C **52**, R23 (1995).
6. G. Audi, A.H. Wapstra, C. Thibault, Nucl. Phys. A **729**, 337 (2003).
7. G. Audi, M. Wang, A.H. Wapstra, F.G. Kondev, M. MacCormick, X. Xu, B. Pfeiffer, Chin. Phys. C **36**, 1287 (2012).
8. M. Bender, P.-H. Heenen, P.-G. Reinhard, Rev. Mod. Phys. **75**, 121 (2003).
9. S. Goriely, S. Hilaire, M. Girod, S. Péru, Phys. Rev. Lett. **102**, 242501 (2009).
10. J.-F. Berger, M. Girod, D. Gogny, Comp. Phys. Commun. **63**, 365 (1991).
11. F. Chappert, M. Girod, S. Hilaire, Phys. Lett. B **668**, 420 (2008) and references therein.
12. J. Libert, M. Girod, J.-P. Delaroche, Phys. Rev. C **60**, 054301 (1999).
13. J.-P. Delaroche, M. Girod, J. Libert, H. Goutte, S. Hilaire, S. Péru, N. Pillet, G.F. Bertsch, Phys. Rev. C **81**, 014303 (2010).
14. S. Hilaire, M. Girod, Eur. Phys. J. A **33**, 237 (2007).
15. F. Chappert, PhD thesis (2007).
16. T.R. Rodríguez, A. Arzhanov, G. Martínez-Pinedo, Phys. Rev. C **91**, 044315 (2015).
17. I. Angeli, K.P. Marinova, At. Data Nucl. Data Tables **99**, 69 (2013).
18. B. Friedman, V.R. Pandharipande, Nucl. Phys. A **361**, 502 (1981).
19. M. Baldo, P. Schuck, X. Viñas, Phys. Lett. B **663**, 390 (2008).
20. Z.H. Li, H.-J. Schulze, Phys. Rev. C **78**, 028801 (2008).
21. X.R. Zhou, G.F. Burgio, U. Lombardo, H.-J. Schulze, W. Zuo, Phys. Rev. C **69**, 018801 (2004).
22. G.F. Bertsch, T.T.S. Kua, Nucl. Phys. A **112**, 204 (1968).
23. V. Bernard, N. Van Giai, Nucl. Phys. A **348**, 75 (1980).
24. M. Bender, G.F. Bertsch, P.-H. Heenen, Phys. Rev. C **73**, 034322 (2006).
25. L.M. Robledo, G.F. Bertsch, Phys. Rev. C **84**, 054302 (2011).
26. L.M. Robledo, Phys. G: Nucl. Part. Phys. **42**, 055109 (2015).
27. A. Akmal, V.R. Pandharipande, D.G. Ravenhall, Phys. Rev. C **58**, 1804 (1998).
28. T. Lesinski, K. Bennaceur, T. Duguet, J. Meyer, Phys. Rev. C **74**, 044315 (2006).
29. W. Zuo, U. Lombardo, H.-J. Schulze, Z.H. Li, Phys. Rev. C **74**, 014317 (2006).
30. S. Raman, C.W. Nestor, P. Tikkanen, At. Data Nucl. Data Tables **78**, 1 (2001).
31. G.F. Bertsch *et al.*, Phys. Rev. Lett. **99**, 032502 (2007).
32. M. Martini, S. Péru, S. Hilaire, S. Goriely, F. Lechaftois, Phys. Rev. C (2016) submitted.
33. D.H. Youngblood *et al.*, Phys. Rev. Lett. **82**, 691 (1999).
34. B.L. Berman, S.C. Fultz, Rev. Mod. Phys. **47**, 713 (1975).
35. M.N. Harakeh, A. Van der Woude, in *Giant Resonances: Fundamental High-energy Modes of Nuclear Excitation* (Oxford University Press, Oxford, 2001).
36. J. Dobaczewski, A.V. Afanasjev, M. Bender, L.M. Robledo, Yue Shi, Nucl. Phys. A **944**, 388 (2015).
37. R. Rodríguez-Guzmán, L.M. Robledo, Phys. Rev. C **89**, 054310 (2014).
38. N. Dubray *et al.*, *Microscopic description of the fission: Automatic production of continuous potential energy surfaces*, `http://www-dam.cea.fr/CG2015/docs/All/Dubray.pdf`.